Analysis of Entropy Generation for the Performance Improvement of a Tubular Solid Oxide Fuel Cell Stack

Chiara Ciano[1*], Michele Calì, Vittorio Verda

Department of Energy Engineering, Politecnico di Torino, Turin, Italy,

Email:[1]chiara.ciano@polito.it

Abstract

The aim of the paper is to investigate possible improvements in the design and operation of a tubular solid oxide fuel cell. To achieve this purpose, a CFD model of the cell is introduced. The model includes thermo-fluid dynamics, chemical reactions and electrochemistry. The fluid composition and mass flow rates at the inlet sections are obtained through a finite difference model of the whole stack. This model also provides boundary conditions for the radiation heat transfer. All of these conditions account for the position of each cell within the stack. The analysis of the cell performances is conducted on the basis of the entropy generation. The use of this technique makes it possible to identify the phenomena provoking the main irreversibilities, understand their causes and propose changes in the system design and operation.

Keywords: Tubular SOFC, fuel cell modelling, configuration analysis, entropy generation.

1. Introduction

In the last decades fuel cells have undergone serious investigation both in the academic and the industrial sectors. In this paper, tubular solid oxide fuel cells (SOFC) are investigated. This is a promising technology for decentralized power generation and cogeneration.

To obtain the desired current and voltage, several cells are connected in series and in parallel. A group of cells is called the stack. Since the electrochemical reaction is exothermic and there is additional energy release due to Joule heating, it is possible to take advantage of this energy release to feed some units where reforming occurs when the system operates with natural gas.

The aim of this paper is to investigate possible improvements in system performance through changes in the stack configuration. An analysis of the different contributions to entropy generation is performed for this purpose. A detailed model is introduced in order to calculate the entropy generation as well as system performance for the configurations analyzed. The whole model consists of two parts: a model of a single cell and a model of the complete stack. The simulations can be performed in two different ways depending on the purpose: 1) to use the results produced by the stack model to set proper boundary conditions and to calculate some of the source terms for the cell model, e.g. the radiation heat fluxes; 2) to use the results produced by the cell model to set some terms in the stack model, e.g. the convection terms. The second approach is used in the present work.

2. Cell Model

The model of the single fuel cell has been developed using the software package Comsol Multiphysics®. The following physical phenomena are taken into account: mass transport, heat transfer, current transport, and electrochemical reactions.

The model consists of a set of partial differential equations and several constitutive equations in order to represent the various phenomena. The partial differential equations in the various domains are the continuity equation for gas mixtures, the momentum equation, energy conservation, the conservation of species written for all components of the gas mixtures minus one, and current conservation.

For air and fuel channels, the momentum equation is written in the form of the general Navier-Stokes equation,

$$\mathbf{u} \cdot \nabla \cdot (\rho \mathbf{u}) = -\nabla p + \mu \nabla^2 \mathbf{u} + \mathbf{S_d} \qquad (1)$$

where the source term $\mathbf{S_d}$ is set to zero. As for the porous media, Brinkman's equation is used (Nield and Bejan, 1999). In it, viscosity effects are taken into account and the equation is as follows:

$$\nabla p = \mu \nabla^2 \mathbf{u} + \frac{\mu}{K} \mathbf{u} \qquad (2)$$

where K is the permeability of the medium considered.

The continuity equation is written as:

$$\nabla \cdot (\rho \mathbf{u}) = 0 \qquad (3)$$

Mass variations are set as boundary conditions on the surfaces where reactions take place. Outgoing fluxes for oxygen are imposed between the cathode and electrolyte; hydrogen and carbon monoxide are set as outgoing fluxes between the anode and electrolyte whereas incoming fluxes are imposed for steam and carbon dioxide on the same surface.

The mass transfer is written by considering the gas species and the mixture of gases. The species equation for the generic species A is then written as:

$$\nabla \cdot (\rho \mathbf{u} w_A) = \nabla \cdot (D_A \rho \nabla w_A) \qquad (4)$$

where w_A is the mass fraction of component A, and D_A is the diffusion coefficient of species A in the mixture (Suwanwarangkul et al., 2003). The change in composition is treated in the species conservation model again considering outgoing and incoming fluxes through the boundaries between the electrodes and the electrolyte.

Eq. 4 is written for n-1 species. The mass fraction of the nth species is calculated as:

$$w_n = 1.0 - \sum_{i=1}^{n-1} w_i \tag{5}$$

The energy equation is in the form

$$\rho \mathbf{u} \cdot \nabla T = \nabla \cdot (\lambda \nabla T) + \varphi_V + \mu \Phi \tag{6}$$

where λ is the global thermal conductivity and φ_V the heat generated per unit volume due to the Joule effects of the current flowing in the electrodes and electrolyte. Heat generated by electrochemical reactions is set as a non-continuity boundary condition on the surface between the anode and electrolyte. In Eq. (6) the hypothesis of thermal equilibrium between the porous structure and the gas is assumed so that a unique local temperature is considered.

Fuel is assumed to be completely reformed at the anode surface, thus reforming reactions have not been modelled.

Finally, current transport is written as

$$k \cdot \nabla^2 V_\Delta = 0 \tag{7}$$

where k is the general electronic or ionic conductivity of the layer and V_Δ is the ohmic overpotential. The activation losses (Butler-Volmer equation) are accounted for through potential drops between the electrodes and the electrolyte (Melhus and Ratkje, 1996). At the outer boundary of each electrode, a value for the potential is imposed (0 for the cathode boundary and V_N–V_{cell} at the anode boundary).

The Nernst potential is the maximum potential that the cell may achieve in the open circuit condition, i.e. when no current flows through it. The expression for V_N is

$$V_N = \frac{-\Delta G}{2F} \tag{8}$$

where ΔG is the change in the Gibbs free energy of the oxidation reactions. We assume that both hydrogen and carbon monoxide take part in the electrochemical reaction.

A possible alternative to this assumption is to consider the water gas shift reaction occurring at the anode side. Figure 1 shows the difference in mass fractions calculated using two models: 1) water gas shift + electrochemical reaction of the hydrogen only; and, 2) electrochemical reactions of both hydrogen and carbon monoxide. This calculation has been performed using experimental data for the inlet gas composition and the total current.

The quantity in the abscissa is the contribution due to hydrogen to the total current in the second model. This means that the total current is considered as constant, but the contribution of hydrogen is varied from 70% to 100%, while the contribution of CO is varied from 30% to 0% accordingly. The results of the first model do not depend on quantity in the abscissa. These results are considered as exact, since this is the model usually considered in the literature.

When the electrochemical reaction of hydrogen contributes about 72% to the total current, the difference between the two models is close to zero. This result is similar to that obtained by assuming the contributions due to H_2 and CO as being proportional to their partial pressures (Verda and von Spakovsky, 2009). The advantage of this approach is a simpler chemical model.

The model is completed by means of a set of constitutive equations which are detailed as follows. The gas mixture density is calculated via the ideal gas law. Specific heats are assumed to be dependent on the gas temperature.
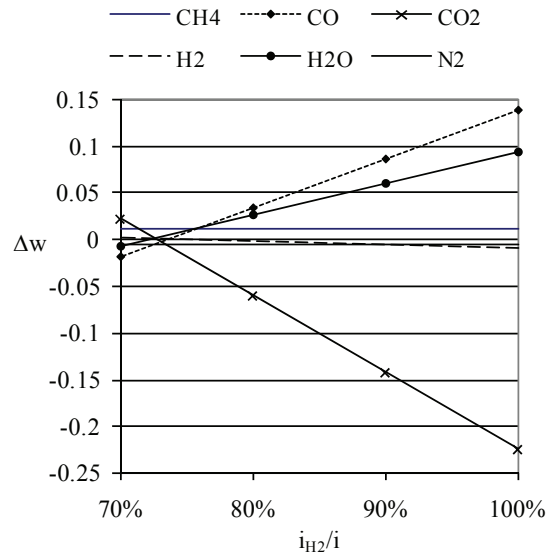
Figure 1. Deviations in Mass Fraction of the Reactants by using Two Different Approaches to the Electrochemical Model.

The species participating in the electrochemical reactions are CO and H_2 at the anode and O_2 at the cathode, i.e.

$$H_2 + O^{2-} \rightarrow H_2O + 2e^- \tag{9}$$

$$CO + O^{2-} \rightarrow CO_2 + 2e^- \tag{10}$$

$$\frac{1}{2} O_2 + 2e^- \rightarrow O^{2-} \tag{11}$$

The ratio between CO and H_2 involved in the electrochemical reactions is assumed as equal to the ratio of the molar fractions of CO and H_2 at the inlet of the fuel channel.

The relationship between the local current density and the consumption of hydrogen, oxygen and carbon monoxide as well as the generation of carbon dioxide and water is expressed using Faraday's law. This means that, in the conservation of species and in the momentum equation models, the term accounting for the outgoing and incoming fluxes through the electrode-electrolyte interface is related to the following equations

$$U_{H_2} = -\frac{i_{H_2}}{2 \cdot F} M_{H_2} \tag{12}$$

$$U_{CO} = -\frac{i_{CO}}{2 \cdot F} M_{CO} \tag{13}$$

$$U_{O_2} = -\frac{i}{4 \cdot F} M_{O_2} \tag{14}$$

$$U_{H_2O} = \frac{i_{H_2}}{2 \cdot F} M_{H_2O} \tag{15}$$

$$U_{CO_2} = \frac{i_{CO}}{2 \cdot F} M_{CO_2} \tag{16}$$

where i_{H2} and i_{CO} are the current densities obtained from the two electrochemical reactions on the anode side. These currents can be obtained from the following relations:

$$i_{H_2} + i_{CO} = i \qquad (17)$$

$$\frac{i_{CO}}{i_{H_2}} = \frac{y_{CO}}{y_{H_2}} \qquad (18)$$

The ionic and electronic resistivities are assumed to be dependent on the temperature according to the equation:

$$\rho = \beta_1 \cdot e^{\frac{\beta_2}{T}} \qquad (19)$$

The values of the selected parameters appear in Table 1 (Campanari and Iora, 2004; Ciano and Verda, 2008).

Table 1. Characteristics of the Cell.

Cell external diameter [m]	22×10^{-3}
Cell length [m]	1.5
Cathode thickness [m]	2.2×10^{-3}
Cathode electric resistivity [$\Omega \cdot$m]	$\beta_1 = 8.11 \times 10^{-5}$ $\beta_2 = 600$
Cathode thermal conductivity [W/K·m]	6
Cathodic exchange current density [A/m^2]	2000
Electrolyte thickness [m]	4×10^{-5}
Electrolyte electric resistivity [$\Omega \cdot$m]	$\beta_1 = 2.94 \times 10^{-5}$ $\beta_2 = 10350$
Electrolyte thermal conductivity [W/K·m]	2.7
Anode thickness [m]	1×10^{-4}
Anode electric resistivity [$\Omega \cdot$m]	$\beta_1 = 2.98 \times 10^{-5}$ $\beta_2 = -1392$
Anode thermal conductivity [W/K·m]	11
Anodic exchange current density [A/m^2]	5300

The cell considered is a tubular SOFC fuelled with a mixture of hydrogen, carbon monoxide, water steam and carbon dioxide. Table 2 gives the composition of the inlet gases and their temperatures and the operating pressure.

Table 2. Air and Fuel Inlet Conditions.

Fuel composition [molar]	55.7% H_2; 27.7% H_2O; 10.8% CO; 5.8% CO_2
Air composition [molar]	21% O_2; 79% N_2
Fuel temperature [°C]	800
Air temperature [°C]	830
Operating pressure [Pa]	1.013×10^5

The main results provided by this model in the specific application are composed of the fluid velocities and the mass fractions of reactants and products. This information is used in the stack model in order to evaluate the convective term in the energy equation and the entropy generation.

Figure 2 shows the mass fraction of reactants on a portion of a longitudinal cross section of 0.3 m length: O_2 on the cathode side (left part of the figure) and CO and H_2 on the anode side. Some streamlines showing the net mass flow rates are also shown. These show that oxygen flows from the channel through the porous cathode towards the cathodic active sites; in contrast, on the anodic site, the net mass flow rate flows from the active sites towards the anodic channel due to H_2O and CO_2 production. The inlet oxygen mass fraction is 0.233 and the outlet mass fraction is 0.227. The inlet hydrogen mass fraction is 0.355 and the outlet hydrogen mass fraction is 0.35.
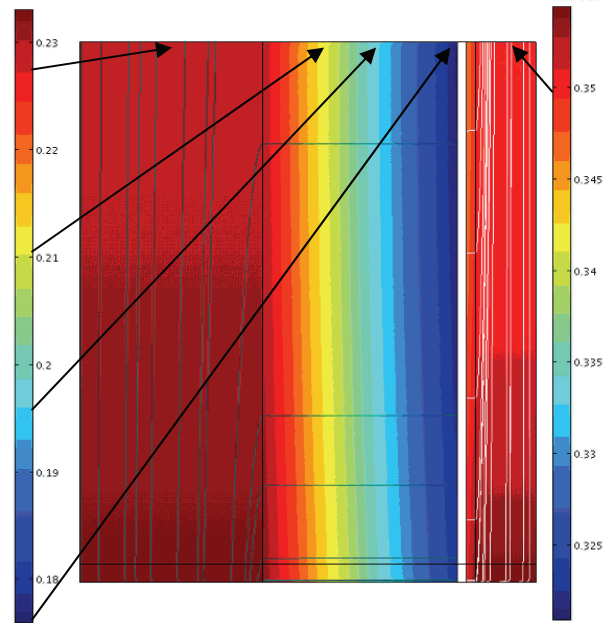
Figure 2. Mass Fraction of Reactants.

When off-design conditions are considered, the temperature and the current change. This affects mainly the concentration of species, which must be determined.

3. Stack Model

The stack considered in this paper consists of 24 cells, whose configuration in rows and series is not fixed. An initial configuration is shown in Figure 3. The cells are arranged in three rows, each composed of 8 cells connected in series. Two external reformers are located on the longer sides of the stack. The reforming reactions occur by taking advantage of heat supplied by the fuel cells.
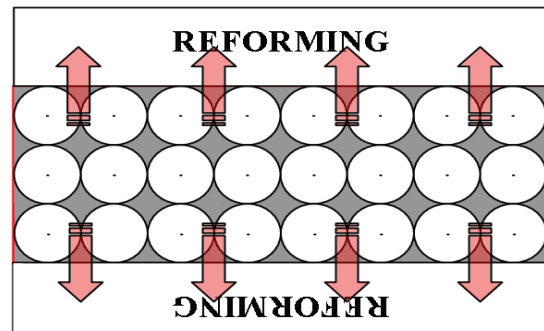
Figure 3. Schematic of the Stack.

Fuel (desulfurized and pre-reformed natural gas) flows through the reformers from the top to the bottom. The gas enters the stack and flows through the channels between the cells, from the bottom to the top. Air flows inside the cells as shown in Figure 4a.
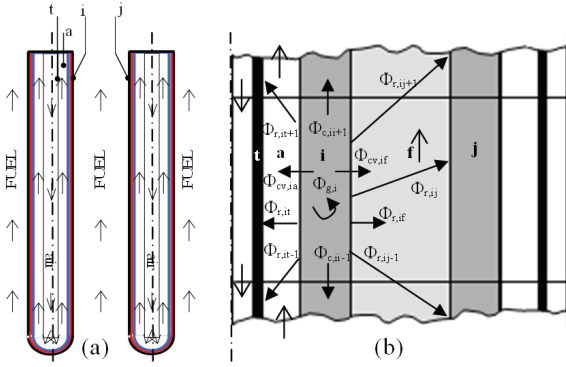
Figure 4: Schematic of a Cell Slice.

In the stack model, the thermal problem and current conservation are solved. The stack is considered as composed of the following elements: cold air, tube (t), hot air (a), cell (i, j), fuel (f). These elements are divided into vertical portions. In addition, the cell elements are split into four circumferential slices. Thermal flows are shown in Figure 4b for a portion of the tubes.

The energy balance of the ith fuel cell slice is expressed:

$$-\Phi_{r,i} - \Phi_{cv,i} - \Phi_{c,i} + \Phi_{g,i} +$$
$$-W_{el} + \sum_{in} J_{in}h_{in} - \sum_{out} J_{out}h_{out} = 0 \quad (20)$$

where $\Phi_{r,i}$ is the net radiative heat transfer, $\Phi_{cv,i}$ is the convective energy transfer which includes the convective heat transfer as well as the enthalpy flows associated with the inlet and outlet flows, $\Phi_{c,i}$ is the conductive heat transfer, $\Phi_{g,i}$ is the heat generated by the electrochemical reactions and the Joule effect, W_{el} is the electric power and the term $J_{in}h_{in}$ accounts for the enthalpy flows of the fluids entering the porous electrodes and $J_{out}h_{out}$ accounts for the enthalpy flows of the fluids exiting the porous electrodes. J is the mass flow rate and h_i is the enthalpy of the gas, which includes both the physical and chemical components. The enthalpies of the exiting flows are evaluated at the same temperature as the cell. A similar equation can be written for the cold air, tube, hot air and fuel.

Radiation is treated by means of a zone model (Hottel and Sarofim, 1967). Additional details about the application of such an approach to the stack model can be found in Ciano et al. (2006). The net radiation heat flux is written as

$$\Phi_{r,i} = \sum_{k=f-1}^{f+1} \Phi_{r,ik} + \sum_{k=t-1}^{t+1} \Phi_{r,ik} + \sum_{\lambda=1}^{ns} \sum_{k=j-1}^{j+1} \Phi_{r,ik} \quad (21)$$

The first term accounts for the heat transfer between the cell and fuel (this term is usually negligible), the second term for the heat transfer between the cell and tube, and the last term for the heat transfer between the cell and the surrounding cells or the reformer. For a cell slice overlooking the center of the bundle, the summation in λ has three terms (ns=3) corresponding to the three cell slices

surrounding the ith slice. For a cell slice overlooking the reformer, the summation has the two terms (ns=2) corresponding to the cell slice adjacent to the ith slice and the reformer surface.

Radiation heat transfer is assumed to be significant between each portion of the cells and the elements in the same plane, in the upper plane and in the lower plane. For this reason, summations in k have three terms. The error associated with this assumption increases when small vertical portions are considered. Figure 5 shows the various view factors as functions of the length of the cell slice (vertical discretization). The four view factors have the following meaning: 1) Fap – view factor between a cell and the 2 adjacent cells in the same horizontal plane; 2) Fop – view factor between opposite cells in the same horizontal plane; 3) Fad - view factor between a cell and the 2 adjacent cells in the upper and lower plane; 4) Fod – view factor between opposite cells in the same horizontal plane. When the element length is larger than 0.04 m, the error is less than 3%.

The convective term appearing in Eq. 20 accounts for the convective heat transfer between surface and fluid. In the case of the exchange between a cell and the fuel:

$$\Phi_{cv,if} = \alpha \cdot A_{ext,i} \cdot \left(T_i - T_f\right) \quad (22)$$

where α is the convective heat transfer coefficient and $A_{ext,i}$ is the external heat transfer area for the cell.
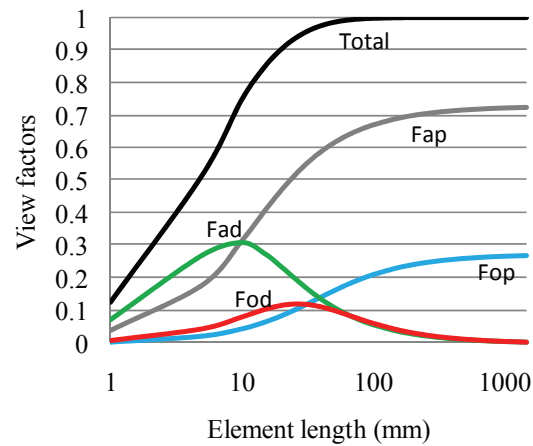
Figure 5. View Factors.

Conductive fluxes are calculated by expressing the Laplace equation in cylindrical coordinates (Incropera and DeWitt, 2002) and by using a finite difference scheme. Furthermore, a finite difference model has also been developed to calculate the electronic/ionic currents in the cells.

The equation of current conservation is expressed using a network model, which relates the overpotentials in some nodes. Using the notation shown in Figure 6, current conservation for the node c,i can be written as:

$$\frac{V_{\Delta c,i} - V_{\Delta c,e}}{R_r} + \frac{2 \cdot V_{\Delta c,i} - V_{\Delta r,i} - V_{\Delta l,i}}{R_c} +$$
$$+ \frac{2 \cdot V_{\Delta c,i} - V_{\Delta t,i} - V_{\Delta b,i}}{R_a} = 0 \quad (23)$$

where R_r, R_c and R_a are the radial, circumferential and axial resistance, V_Δ is the overpotential, and subscripts *c, t, b, l, r,*

i, *e* mean center, top, bottom, left, right, internal, external. The radial resistivity accounts for the electronic resistivity of both electrodes, the ionic resistivity of the electrolyte and the activation overpotentials at the interfaces between electrodes and electrolyte. The circumferential and axial resistivities account for the electronic resistivities of the cathode only, as it is much thicker than the other layers.
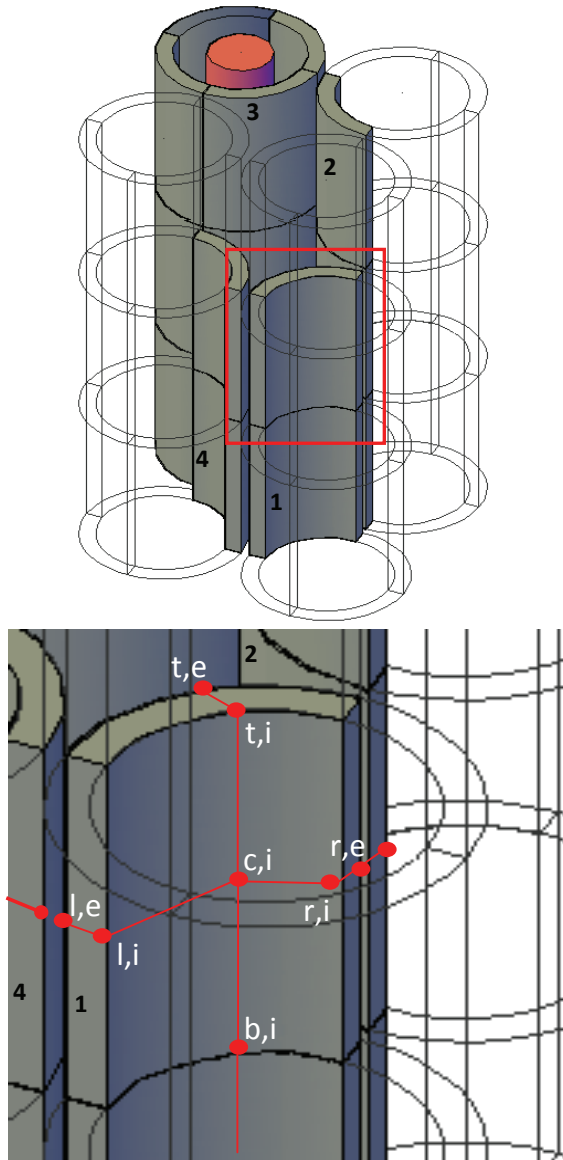
Figure 6. Network Model for the Conservation of Current.

Figure 6 also shows that node r,e of cell number 1 is connected with the node on the interior surface of cell number 2. The two cells are connected in series. In contrast, the node l,e of cell number 1 is not connected with the corresponding node of cell number 4. This is because the two cells are in parallel.

4. Results

Entropy generation is calculated by using the model of the whole stack. Only the terms related to fluid dynamics and the distribution of species are calculated by using the single cell model.

Such an analysis highlights the contribution of each source of irreversibility to the total entropy generation, as well as the distribution of each source within the system.

Entropy generation can be calculated by considering the following expression:

$$\dot{s}_g = -\frac{\varphi \cdot \nabla T}{T^2} + \frac{i \cdot \nabla V_\Delta}{T} + \frac{\Phi_r}{V}\left(\frac{1}{T} - \frac{1}{T^*}\right) + \frac{\varphi_V}{T} +$$
$$\rho \cdot u \cdot \nabla s + \frac{\mu \Phi}{T} - \frac{\sum \left(J_j / A\right) \cdot \nabla \mu_j}{T} + \frac{\sum r_j \cdot \mu_j}{T} \qquad (24)$$

The first term represents the contribution of heat conduction, the second term is the entropy generated by current transfer (ohmic losses), the third term is related to radiative heat transfer and the fourth term to volumetric heat generation (in this work it accounts for the entropy generation due to activation losses); the fifth term is the convective term, the sixth term accounts for fluid friction and the last two terms are related to the chemical/electrochemical reactions (Bejan, 1996; Sarmiento-Darkin and Lior, 2005; Dunbar et al., 1992). The expression for entropy generation can be obtained, as in Bejan (1996), by writing the second law for a continuum and substituting in it the expression of heat flux obtained from the first law. In the case of fuel cells, the term $i \cdot \nabla V_\Delta$ appears in the expression of the first law. The term related to radiation heat transfer has been calculated through the finite difference model; its contribution is calculated by combining together the second law written for the emitting surface/volume (whose general temperature is indicated as T*) and for the receiving surface/volume at temperature T (Bejan, 1996). The entropy generation has been considered as concentrated in the element receiving the net flux, whose volume is V. Properties of the various reactants have been calculated by using the expressions available in Gyftopoulos and Beretta (2005).

The contribution of the terms is shown in Figure 7. The numbers in brackets refer to the terms in Eq. 25. The term associated with the electrochemical reaction is the largest, but it is practically intrinsic. An effective way to reduce this contribution consists in modifying the fuel cell geometry in order to increase the active surface, as shown in Sciacovelli and Verda (2008). The present work is focused on the design of a stack made up of available fuel cells, thus this option is not considered.
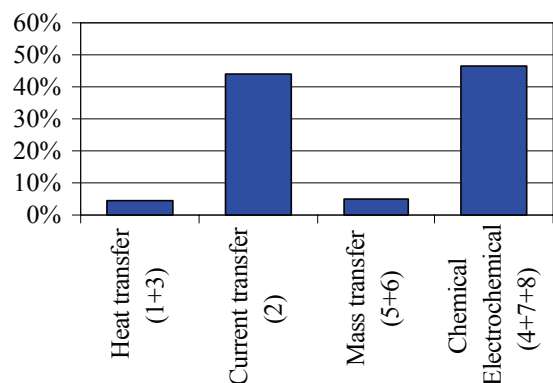
Figure 7. Terms of the Entropy Generation

Figure 8 shows the ratio between the entropy generation associated with the electrochemical reactions at the given operating condition and that at the design condition (900 °C). For a single fuel cell, the entropy generation due to electrochemical reactions at the design condition is about 0.1175 kW/K. Note that it is possible to reduce this term only by a small percentage by reducing the cell operating

temperature. However, temperature has a direct effect on cell resistivity and, thus, on ohmic losses, which represent about 45% of the total entropy production in the cell (this is the contribution indicated as current transfer in Figure 7).
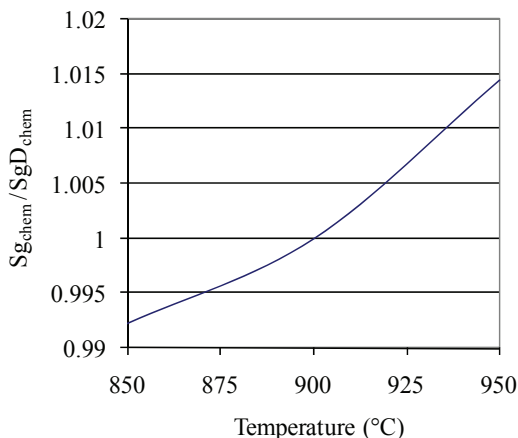
Figure 8. Effect of Temperature on the Entropy Generation due to Electrochemical Reactions.

The average ohmic resistance of the cell as a function of its temperature is shown in Figure 9. On the same figure, the entropy generation in a fuel cell as a function of the average operating temperature is shown. An increase in the operating temperature causes a significant reduction in the entropy generation due to ohmic losses (Second term in Eq. 24). This is due to the reduction in the numerator, which is proportional to the resistance if a constant current density is assumed, and an increase in the denominator. If the operating temperature of the fuel cell were increased from 900 °C to 925 °C the convective term of entropy generation in a single cell increases from 0.1175 kW/K to 0.1184 kW/K. In contrast, the term associated with ohmic losses decreases from 0.1110 kW/K to 0.0941 kW/K. This means that the total entropy generation is expected to reduce about 6%. In this calculation the effect of the temperature on the other entropy generation terms has been neglected, as these terms only contribute about 12% to the total entropy generation.
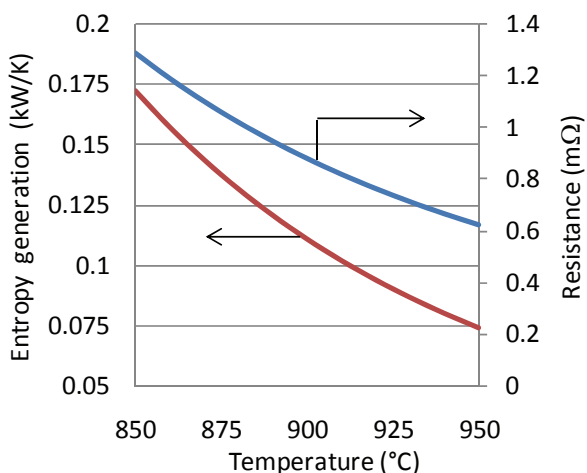
Figure 9. Ohmic Resistance of the Cell and Corresponding Entropy Generation.

An interesting way to improve fuel cell performance consists in changing the stack design so that a different cell temperature distribution is obtained.

Figure 10 shows the temperature distribution for the basic configuration. Air enters at about 830 °C from the top (24 inlet points are shown in the top plane), while fuel enters from the bottom at about 900 °C. These boundary conditions are not affected by the configuration.
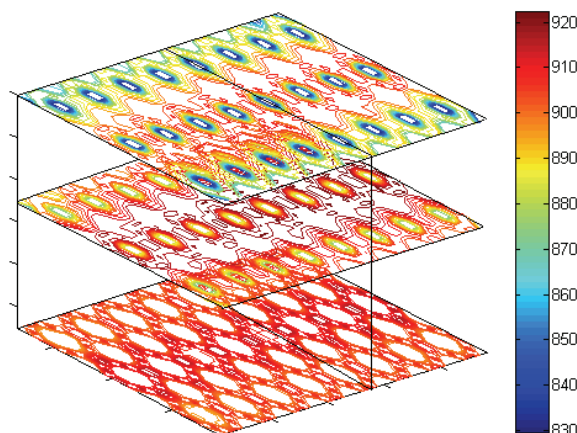
Figure 10. Temperature Distribution (Basic Configuration).

The most significant temperatures are related with two cells, one at the boundary (plain lines) and one in the center (dashed lines) of the vertical section, are shown in Figure 11.
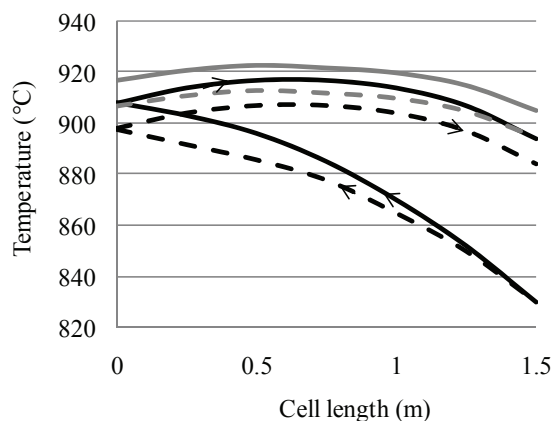
Figure 11. Cell Temperature (Basic Configuration)

Grey curves refer to the average cell temperature, while black curves refer to the air temperature, which has a U-shape flow (arrows on the black curves indicate the direction of the air flow). The temperature of the cell in the center is higher than the cell at the boundary. The difference is due to the heat flux exchanged between the cells and the reformers in the y direction. This also means that the current produced by the cell in the center is larger (about 145 A/cell) than the current produced by the boundary cell (about 132 A/cell).

An improvement should be obtained by arranging the cells in four rows. In this way, the average temperature of the inner cells increases and also the number of cells in this zone increases. This is shown in Figures 12 and 13. The decreased temperature of the boundary cells, due to the constant heat flux required by the reformers, produces a performance degradation in these cells less important than the efficiency increase of the inner cells.

The current in the inner cells is about 156 A/cell, while in the boundary cells it is about 129 A/cell. If the four rows are connected in parallel, the bundle voltage decreases by

25% due to the reduced number of cells in series. In contrast, the total current increases by about 35%. In this way the total power of the bundle increases by about 4%. This has a positive impact on the cost per kW of the fuel cell stack.

If the configuration were changed in the direction of increasing the number of cells exchanging heat with the reformer, the total power would increase. Nevertheless, this would result in a large temperature gradient in the boundary cell that might be unacceptable.
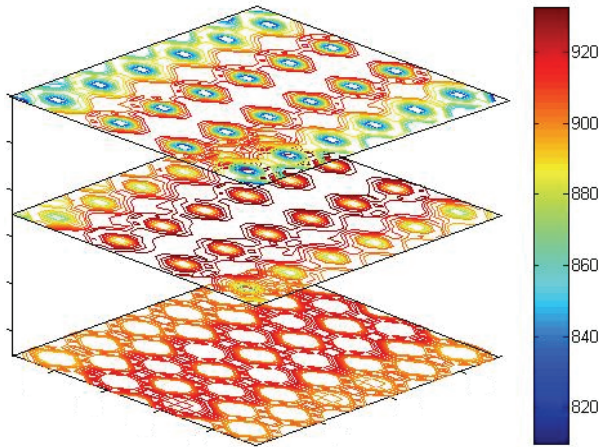
Figure 12. Temperature Distribution (Improved Configuration)
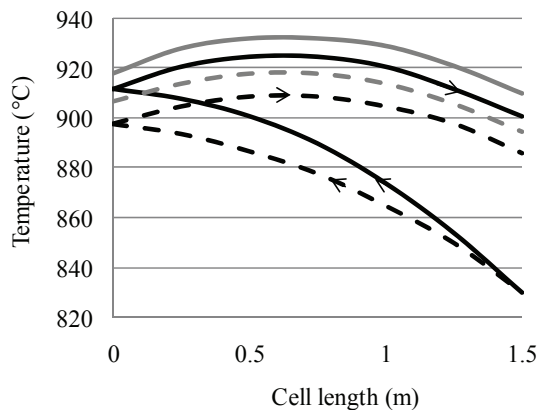
Figure 13. Temperature Distribution (Improved Configuration)

5. Conclusions

In this paper, the configuration of the stack of a solid oxide fuel cell generator is analyzed with the aim of investigating possible improvements in stack performance. It is shown that an optimization of the stack configuration would produce a significant increase in the power density and thus a reduction in stack costs. This kind of improvement should also involve a redesign of the whole system (stack plus balance of plant). In particular the operating conditions of the cells and of the other components (the reformer, the afterburner and the heat exchangers) should be investigated. Current work is focused on this topic.

Nomenclature

A	Surface [m^2]
D	Diffusion coefficient [m^2/s]
E_a	Activation energy [J/mol]
F	Faraday's constant [C/mol]
G	Gibbs free energy [J/mol]
h	Specific enthalpy [J/kg]
i	Current density [A/m^2]
J	Mass flow rate [kg/s]
k	Effective conductivity [$1/(\Omega \cdot m)$]
K	Permeability [m^2]
M	Molar mass [kg/kmol]
p	Pressure [Pa]
r	Reaction rate [$kg/(m^3 \cdot s)$]
R	Rlectric resistance [Ω]
S_d	Source term in the momentum equation [$kg/(m^2 \cdot s^2)$]
T	Temperature [K]
T*	Temperature of the general surface exchanging radiant heat with the ith surface [K]
u	Velocity [m/s]
U	Boundary source terms in the momentum equation and in the conservation of species [$kg/(m^2 \cdot s)$]
V	Volume [m^3]
V_{cell}	Cell potential [V]
V_N	Nernst potential [V]
V_Δ	Ohmic overpotential [V]
w	Mass fraction
W_{el}	Electric power [W]
y	Molar fraction

Greek

α	Convective heat transfer coefficient [$W/m^2 \cdot K$]
λ	Conductivity [$W/(m \cdot K)$]
μ	Dynamic viscosity [$kg/(m \cdot s)$]
$\mu\Phi$	Viscous term in the energy equation [W/m^3]
μ_j	Chemical potential [J/kg]
ρ	Density [kg/m^3]
ρ	Resistivity [$\Omega \cdot m$]
φ	Heat flux per unit surface [W/m^2]
φ_V	Heat flux generated per unit volume [W/m^3]
Φ	Heat flux [W]
$\Phi_{r,i}$	Net radiative heat transfer [W];
$\Phi_{cv,i}$	Convective heat transfer [W];
$\Phi_{c,i}$	Conductive heat transfer [W]
$\Phi_{g,i}$	Heat generated [W]

References

Bejan A., 1996. *Entropy Generation Minimization: The Method of Thermodynamic Optimization of Finite-Size Systems and Finite-Time Processes,* CRC Press. Boca Raton, Fl.

Campanari S., Iora P., 2004, **"Definition and Sensitivity analysis of a finite volume SOFC model for a tubular cell geometry",** *Journal of Power Sources*, 132:113-126.

Ciano C., Calì M., Melhus O., Verda V., 2006, "A Model for the Configuration Design of a Tubular Solid Oxide Fuel Cell Stack", ASME Paper, *IMECE2006-16141*, Chicago, IL, November 5-10.

Ciano C., Verda V., 2008, **"CFD Modeling of Tubular SOFCs",** *Modeling Solid Oxide Fuel Cells: Methods, Procedures and Techniques (Fuel Cells and Hydrogen*

Energy), eds., Bove, R., and Ubertini, S., pp. 207-238. Springer.

Dunbar W.R., Lior N., Gaggioli R.A., 1992, "The Component Equations of Energy and Exergy", *ASME J. Energy Resources Technology*, Vol. 114, 75-83.

Gyftopoulos E., Beretta G.P., 2005, *Thermodynamics: Foundations and Applications,* Dover Publications, Mineola, NY.

Hottel, H.C., Sarofim, A.F., 1967, *Radiative Transfer*. McGraw-Hill., New York.

Incropera F.P., DeWitt D.P., 2002, *Fundamentals of Heat and Mass Transfer*., Wiley. Hoboken.

Melhus O., Ratkje S.K., 1996, "A Simultaneous Solution of All Transport Properties in a Solid Oxide Fuel Cell", *Dengi Kagaku*, Vol. 64, No. 6, pp. 662-673.

Nield D.A., Bejan A. , 1999, *Convection in Porous Media*, New York, Springer.

Sarmiento-Darkin W., Lior N., 2005, "Methodology for Intrinsic Exergy Analysis as Guide for Process Improvement, with a Fuel Droplet Combustion Example", ASME Paper, *IMECE 2005-80554*. Orlando, Fl, November 5-11.

Sciacovelli A, Verda V., 2008, "Entropy Generation Minimization on a Tubular Solid Oxide Fuel Cell", ASME Paper, *IMECE 2008-68910*, Boston, MA, October 31 - November 6.

Suwanwarangkul R., Croiset E., Fowler M.W., Douglas P.L., Entchev E., Douglas M.A., 2003, "Performance Comparison of Fick's, Dusty-gas and Stefan–Maxwell Models to Predict the Concentration Overpotential of a SOFC Anode", *Journal of Power Sources*, Vol. 122, pp. 9–18.

Verda V, von Spakovsky M.R., 2009, "Development of a Detailed Planar SOFC CFD Model for Analyzing Cell Performance Degradation", *ASME Journal of Fuel Cell Science and Technology*, Vol. 6, Issue 1, 011005.